

Antiwindup Compensation for Unstable Rigid-Body Systems with Quantized and Saturated Inputs

Christopher M. Richards*
University of Louisville, Louisville, Kentucky 40292
and

Matthew C. Turner[†]

University of Southampton, Southampton, England SO17 1BJ, United Kingdom

https://doi.org/10.2514/1.G007724

It is well known that actuator saturation can cause destabilization and degradation in performance; similar problems are encountered when actuation is quantized. This study proposes the design of an antiwindup compensator for systems with actuators that are limited to a finite number of quantization levels. This combination of discrete-level actuation and saturation poses a unique antiwindup problem that has not yet been solved. To surmount this combined issue, an antiwindup compensator is proposed, which provides ultimate boundedness of the system state within a prescribed region and guarantees that the state does not stray outside a larger compact set. The use of shifted ramp functions enables a less conservative bound on the control-signal error, which yields significantly lower \mathcal{L}_2 gain bounds compared to a standard sector-bound antiwindup design approach. A numerical simulation example illustrates the effectiveness on a rigid-body system, which inspired this study.

I. Introduction

QUANTIZER maps a continuous-valued signal to a discrete-valued signal [1] and can result from analog-to-digital converters, digital sensors, and binary actuators, to name a few [2–7]. The issue of quantization was first discussed by Kalman in the 1950s [8]. However, it was not until the 1990s that Delchamps advocated a direct analysis of the effects of quantization on a system [3]. The effects of quantization are similar to those of actuator saturation; they are unpredictable but typically detrimental to a system's behavior [3,8–10], and a system rendered globally asymptotically stable by a control law will not necessarily remain so when quantization is introduced [9]. Prior research has addressed logarithmic quantizers, where quadratic stability analysis was applied [9,11,12]. However, this analysis is not applicable to many practical systems with uniform or nonuniform quantization.

Moreover, some mechanical and aerospace systems experience control signals that are subject to both quantization and saturation. For example, the NASA Lunar Pallet Lander uses a bank of unidirectional binary actuators that, when used in unison, results in quantized input forces to the vehicle [2]. Likewise, because a finite number of actuators are available, saturation results when the thrust demand exceeds the total available thrust. A scenario such as this is typical of a number of practical systems and was the motivation for this study.

The combination of saturation and quantization has not been studied extensively in the literature, with perhaps the most comprehensive treatment given in [13] where conditions were given for state-feedback stabilization of a system subject to input quantization and saturation. Crucially, the conditions ensured that the system state was ultimately bounded, with this set contained within another set that approximated the region of attraction. These conditions made the results of [13] applicable to both stable and unstable systems.

Presented at the American Control Conference, San Diego, CA, May 31–June 2, 2023; received 16 May 2023; revision received 17 January 2024; accepted for publication 13 April 2024; published online 27 May 2024. Copyright © 2024 by the American Institute of Aeronautics and Astronautics, Inc. All rights reserved. All requests for copying and permission to reprint should be submitted to CCC at www.copyright.com; employ the eISSN 1533-3884 to initiate your request. See also AIAA Rights and Permissions www. aiaa.org/randp.

For systems with saturation, it is typical to rewrite the saturation nonlinearity as sat(u) = u - Dz(u) and then use sector bounds on the dead-zone, Dz(u), to arrive at conditions that ensure stability. These conditions can be stated globally for stable plants, and, by using sector-narrowing techniques [14,15], local stability conditions can be obtained for unstable plants. For instance, Fig. 1 shows that when $\psi(u) = Dz(u)$, then for all $u < \check{u}, \ \psi(u) \in \text{sector}[0, \epsilon]$ with ϵ < 1. However, this is not as straightforward for systems suffering from actuator saturation and quantization because the sectornarrowing approach cannot be applied. Using the same split as before yields $sat(q(u)) = u - \pi(u)$, where $\pi(u)$ models the difference between the nominal control signal and its saturated, quantized counterpart. It is clear from Fig. 1 that the narrowest sector that $\pi(u)$ can inhabit is sector [0, 1], regardless of the local bound, \check{u} , on the control signal used. Therefore, when $\psi(u) = \pi(u) =$ $u - \operatorname{sat}(q(u))$, sector narrowing is not possible with the narrowest sector being sector [0, 1], regardless of the size of \check{u} . This is not problematic for stable plants; however, for unstable plants, it effectively prevents any conclusions about stability from being made. Therefore, other approaches must be adopted.

An attractive alternative to standard sector constraints for saturation/quantization nonlinearity can be obtained from the properties of ramp functions that were exploited in a previous study [16] (also more recently in [17,18]) for the analysis of piecewise affine systems. Similar to [16], it can be shown that the quantization/saturation nonlinearity can be more accurately approximated using ramp functions, and that such approximations naturally lead to a set of quadratic constraints that can be used in Lyapunov analysis. These more accurate approximations have the potential to reduce conservatism in the stability analysis and, by imposing a limit on the energy of the input that drives the antiwindup compensator, offer a suitable alternative to sector narrowing in the case of open-loop unstable systems.

The contribution of this study is the advocacy of antiwindup compensation (AWC[‡]) to address the uniform quantization and saturation problem. Antiwindup compensation has been well studied for systems with input saturation (e.g., [19–22]) and assists a nominal *a priori* designed controller during periods of saturation. Although there is some work on applying AWC to input-quantized plants [23,24], the results developed here have gone beyond those of [23,24], where only quantization was considered, and instead have used the ultimate boundedness/local stability ideas of Tarbouriech

^{*}Associate Professor, Department of Mechanical Engineering; chris. richards@louisville.edu.

[†]Professor, School of Electronics and Computer Science; M.C.Turner@soton.ac.uk.

[‡]AWC is used for antiwindup compensation and as an antiwindup compensator. The meaning is clear from the context.

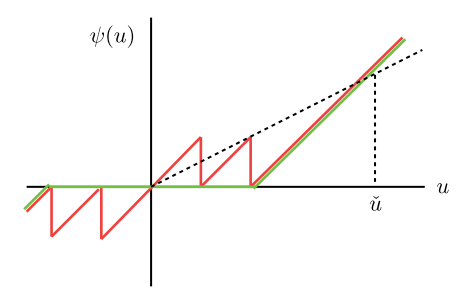


Fig. 1 Sector-narrowing issues with quantization. — $\psi(u) = Dz(u)$; — $\psi(u) = \pi(u) = u - sat(q(u))$.

and Gouaisbaut [13] along with sharper characterizations of the saturation/quantization nonlinearity, inspired by Groff et al. [16]. This provides less conservative quadratic constraints and, as shown from the results, a significant reduction in the \mathcal{L}_2 gain bounds compared with an antiwindup design algorithm using sector [0, I]. The approach blends the practicality of the antiwindup approach and the technical rigor of [13] while reducing conservatism in the design. Crucially, ramp-function characterizations [16] were exploited for AWC synthesis while only requiring the solution of a linear matrix inequality. A preliminary version of this study was presented in [25]. The main additions found in this study include more complete antiwindup derivations and a larger sample of simulation results.

This paper is structured as follows. Section II states the AWC design problem for the quantized and saturated control signals. Section III provides the bounds on the control-signal error $\pi(u)$ and preliminaries for the main result. Section IV discusses the linear performance recovery, stability, and performance analysis and presents the main result. Section V provides and critiques sample simulation results. Section VI draws conclusions and states efforts for future work.

Notation is mainly standard and follows that of [21]. The reader's attention is drawn to the following notation: $\mathbb{R}^{n\times m}$ denotes the set of matrices with real coefficients of dimension n by m. Let $M_{(i,j)}$ denote the element in the (i,j) entry of matrix M, and M_i the ith row of M, denote $\mathbb{D}^n = \{M \in \mathbb{R}^{n\times n} | M_{(i,j)} = 0, i \neq j\}$, $\mathbb{P}^{n\times m} = \{M \in \mathbb{R}^{n\times m} | M_{(i,j)} \geq 0, \forall i,j\}$, and $I_n \in \{\mathbb{D}^n | I_{n(i,i)} = 1\}$. A statespace system

$$\dot{x}(t) = f(x(t)) \quad f(\cdot) : \mathbb{R}^n \mapsto \mathbb{R}^n$$

is described as locally ultimately bounded if for all $x(0) \in \mathcal{X}_1 \subset \mathbb{R}^n$, there exists a time t_1 and a set $\mathcal{X}_2 \subset \mathbb{R}^n$ such that $x(t) \in \mathcal{X}_2$ for all $t \geq t_1$.

II. Problem Statement

This study addresses control signals with a finite number of quantized levels and is inspired by the problem of controlling rigid-body systems with a limited number of quantized thrusters.

Consider m thruster banks made up of n_{T_i} , $i=1,\ldots,m$ bidirectional binary thrusters with equal thrust magnitudes δT_i . Then, the control signal u is subject to quantization with saturation described by $\phi(u) = \operatorname{sat}_{\bar{u}}(q(u)) = [\operatorname{sat}_{\bar{u}_1}(q_1(u_1)) \ldots \operatorname{sat}_{\bar{u}_m}(q_m(u_m))]'$, where

$$\operatorname{sat}_{\bar{u}_i}(q_i(u_i)) \coloneqq \begin{cases} -\bar{u}_i & \text{if} \quad q_i(u_i) \leq -\bar{u}_i \\ q_i(u_i) & \text{if} \quad -\bar{u}_i < q_i(u_i) < \bar{u}_i \\ \bar{u}_i, & \text{if} \quad q_i(u_i) \geq \bar{u}_i \end{cases}$$

and $\bar{u}_i = n_{T_i} \delta T_i$. Symmetric actuation is assumed throughout; amendments may be made to deal with asymmetric actuators by allowing the upper and lower bounds on the saturation function to differ.

To manage the effects of quantization plus saturation on the control signal, the antiwindup architecture shown in Fig. 2 is considered, where G(s), K(s), and $\Theta(s)$ are the plant, controller, and AWC, respectively, with state-space realizations:

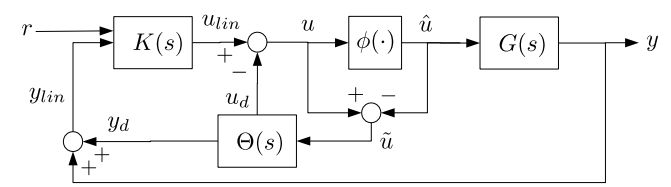


Fig. 2 Antiwindup architecture: $\phi(u)$, quantization and saturation nonlinearity; $\Theta(s)$, AWC.

$$G(s) \sim \begin{cases} \dot{x}_p = A_p x_p + B_p \phi(u) \\ y = C_p x_p \end{cases} \tag{1}$$

$$K(s) \sim \begin{cases} \dot{x}_c = A_c x_c + B_c (y + y_d) + B_{cr} r \\ u_{lin} = C_c x_c + D_c (y + y_d) + D_{cr} r \end{cases}$$
 (2)

$$\Theta(s) \sim \begin{cases} \dot{x}_a = (A_p + B_p F) x_a + B_p \tilde{u} \\ u_d = F x_a \\ y_d = C_p x_a \end{cases}$$
 (3)

where the control signal is $u = u_{\text{lin}} - u_d \in \mathbb{R}^m$, the measured output is $y \in \mathbb{R}^p$, and the reference input is $r \in \mathbb{R}^{n_r}$. The plant is driven by the quantized and constrained signal $\hat{u} = \phi(u)$, and the AWC is driven by the difference between the control signal and its quantized and constrained counterpart $\tilde{u} = \pi(u) = u - \phi(u)$, which is referred to as the *control-signal error*. The AWC, which has a typical antiwindup structure as, for example, found in [19,23], emits two signals: $u_d \in \mathbb{R}^m$ and $y_d \in \mathbb{R}^p$. It is assumed that in the absence of quantization/saturation, the controller K(s) stabilizes G(s) and provides satisfactory performance. The objective is to design the AWC, specifically F, such that in the presence of quantization/saturation, the closed-loop system is stable, and satisfactory performance, as defined in Sec. IV, is maintained.

Remark 1: The quantized and saturated closed-loop system is represented by a set of differential equations with a discontinuous right-hand side and thus may not admit classical solutions. In this study, as in [13], unique Carathéodory solutions are assumed to exist to these differential equations, and in this sense, the closed loop is said to be well posed. Obviously, this excludes sliding mode and other types of behavior; the interested reader may consult [26] for a general coverage of the subject of discontinuous control systems, or [27] for a differential inclusion formulation.

III. Preliminaries for the Main Result

Motivated by the piecewise nature of the control-signal error, this study extensively uses shifted ramp functions [16] to obtain tighter quadratic constraints than are possible using sector bounds. A shifted ramp function is given by

$$r_{s_i}(u_i) := \begin{cases} 0 & \text{if} \quad u_i < s_i \\ u_i - s_i & \text{if} \quad u_i \ge s_i \end{cases}, \ i = 1, \dots, m$$

The vector-valued decentralized shifted ramp function is

$$r_s(u) \coloneqq [r_{s_1}(u_1) \dots r_{s_m}(u_m)]'$$

For a single thrust control signal, the control-signal error \tilde{u}_i is bounded by

$$|\tilde{u}_i| \le |u_i - r_{\delta T_i}(u_i) + r_{(n_{T_i} + 1)\delta T_i}(u_i) + r_{-\delta T_i}(u_i) - r_{-(n_{T_i} + 1)\delta T_i}(u_i) + \bar{u}_i|$$
(4)

For asymmetric quantization or quantization of differing levels, Eq. (4) would need to be substituted with a different expression but one that is similar in nature. This has repercussions on the main result, but parallel derivations would yield similar results.

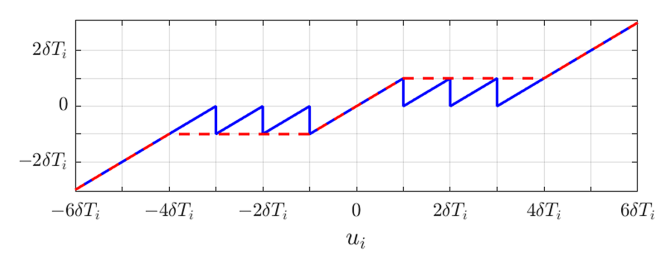


Fig. 3 Control-signal error bound: —, control-signal error \tilde{u}_i ; —, bound $u_i - r_{\delta T_i} + r_{4\delta T_i} + r_{-\delta T_i} - r_{-4\delta T_i} + 3\delta T_i$.

Figure 3 illustrates Eq. (4) for a thruster bank with three thrusters $(n_{T_i}=3)$ of equal thrust magnitudes δT_i . For a more compact notation, we define $r_{a_i} \coloneqq r_{\delta T_i}(u_i), r_{a_i} \coloneqq r_{-\delta T_i}(u_i), r_{b_i} \coloneqq r_{(n_{T_i}+1)\delta T_i}(u_i),$ and $r_{b_i}^- \coloneqq r_{-(n_{T_i}+1)\delta T_i}(u_i)$. Then, for $W \in \mathbb{D}^{m \times m} > 0$, and since $\mathrm{sign}(\tilde{u_i}) = \mathrm{sign}(u_i)$ and $|\tilde{u}_i| \le |u_i|$, the following quadratic inequality holds:

$$\tilde{u}'W(u - r_a + r_b + r_a^- - r_b^- + \bar{u} - \tilde{u}) \ge 0$$
 (5)

For unstable or marginally stable systems with poles that lie at the origin of the complex plane (the latter being pertinent for the rigid-body systems considered here), global stability properties, such as finite \mathcal{L}_2 gain, are difficult or impossible to obtain. Thus, it is necessary to confine attention to a region of the state space surrounding the origin. Notice from Fig. 3 that

$$|u_i - r_{a_i} + r_{b_i} + r_{a_i}^- - r_{b_i}^- + \bar{u}_i| - |\tilde{u}_i| \le |\delta T_i|, \forall u_i$$

Therefore, the following holds:

$$\tilde{u}'W(u - r_a + r_b + r_a^- - r_b^- + \bar{u} - \tilde{u} + Hx_a) \ge 0$$
 (6)

 $\forall x_a \text{ satisfying } \operatorname{sat}_{\delta T}(Hx_a) = Hx_a.$ To ensure $\operatorname{sat}_{\delta T}(Hx_a) = Hx_a$, we impose a limit on the energy of the input u_{lin} , which drives the AWC (see Fig. 2 and discussion in Sec. IV). If it is true that there exists a positive definite function $V(x_a) = x_a' P_1 x_a$ such that $\dot{V}(x_a) \leq 2u'_{\text{lin}} u_{\text{lin}}$ whenever $x_a' P_1 x_a \leq s^2$ and $\|u_{\text{lin}}\|_2 \leq s/\sqrt{2}$, s < 1, then by integrating $\dot{V}(x_a)$

$$V(x_a) \le 2||u_{\text{lin}}||_2^2 \le s^2$$

Therefore, the following condition is imposed:

$$s^2 x_a' H_i' H_i x_a / \delta T_i^2 < x_a' P_1 x_a \tag{7}$$

for all $x_a \neq 0$ and all $i \in \{1, ..., m\}$. Thus, when the control signal satisfies the energy condition and the state remains in the ellipsoid defined by P_1 and s^2 , the sectorlike bound (6) can be used in the ensuing Lyapunov analysis.

To establish the feasible linear matrix inequalities introduced in the next section, the following properties of the shifted ramp functions are used:

1) Null property, $r_{a_i}(r_{a_i} - (u_i - a_i)) = 0$, i = 1, ..., m. Therefore, for $T_a, T_b \in \mathbb{D}^m$

$$r'_a T_a (r_a - (u - a)) = 0, \quad r'_b T_b (r_b - (u - b)) = 0$$

2) Null property, $(u_i - a_i) - (r_{a_i} - r_{a_i}^-) = 0, i = 1, \dots, m$. Therefore, for any $\zeta \in \mathbb{R}^{n_{\zeta}}$ and $R_a, R_b \in \mathbb{R}^{n_{\zeta} \times m}$

$$\zeta' R_a (u - a - r_a + r_a^-) = 0, \quad \zeta' R_b (u - b - r_b + r_b^-) = 0$$

3) Positivity property, $r_{a_i} \geq 0, r_{a_i} \geq 0, r_{a_i} r_{b_i} \geq 0, r_{a_i} r_{b_i} \geq 0, r_{a_i} r_{b_i} \geq 0$, where $i = 1, \ldots, m$. Therefore, for $\chi = [1r'_a r_a^{-\prime} r'_b r_b^{-\prime}]'$ and $M \in \mathbb{P}^{n_\chi \times n_\chi}, n_\chi = 1 + 4m$

$$\chi' M \chi \ge 0$$

In the following section, the conditions for the "stability" of the system comprising the plant, controller, antiwindup compensator, and saturation/quantization nonlinearity are formulated. It will be shown that part of this problem can be cast as that of guaranteeing local ultimate boundedness of the AWC state. Therefore, similar to [13], the following sets are introduced:

$$\mathcal{E}(P_1) = \{ x_a \in \mathbb{R}^n; x_a' P_1 x_a \le 1 \}, P_1 = Q_1^{-1}$$
(8)

$$\mathcal{E}(P_2) = \{ x_a \in \mathbb{R}^n; x_a' P_2 x_a \le 1 \}, P_2 = Q_1^{-1} Q_2 Q_1^{-1}$$
 (9)

where P_1, Q_1, P_2 , and Q_2 are positive definite matrices, which are introduced shortly. $\mathcal{E}(P_2)$ represents the set of ultimate boundedness, whereas $\mathcal{E}(P_1)$ represents a larger set such that for all $x_a(0) \in \mathcal{E}(P_1)$, then $x_a(t)$ will converge to a region containing $\mathcal{E}(P_2)$ in finite time.

Remark 2: For unstable plants, these sets are necessary to obtain meaningful stability results. For stable plants, they are not necessary but may improve local performance.

IV. Main Result

The antiwindup approach proposed in this study mirrors that of [19] in that conditions are sought to guarantee that the system is "stable" (in the sense discussed in Remark 3) and that the mismatch between the ideal linear system, without saturation and quantization, and the real nonlinear system is minimized in some sense. This mismatch system ([19]; see also [15,28]) is governed by the dynamics:

$$\mathcal{N} \sim \begin{cases} \dot{x}_a = (A_p + B_p F) x_a + B_p \tilde{u} \\ u = u_{\text{lin}} - F x_a \\ y_d = C_p x_a \end{cases}$$
 (10)

where the difference between the ideal linear output y_{lin} and the actual output y is y_d . This scenario is depicted in Fig. 4. Thus, for satisfactory behavior, the goal is to synthesize the AWC gain F such that Eq. (10) is stable and the \mathcal{L}_2 gain from u_{lin} to y_d is bounded by a constant γ .

Remark 3: The reader should understand "stability" in a slightly generalized sense similar to that considered in [13]. In particular, and with some abuse of terminology, $\mathcal N$ will be described as "stable" if, for $u_{\text{lin}} \equiv 0$, $x_a(t)$ converges to the smallest level set containing $\mathcal E(P_2)$ for all $x_a(0) \in \mathcal E(P_1)$ in finite time. Similarly, because $\tilde u(t)$ will generally not converge to zero (because the quantization is "active" all the time), a true $\mathcal L_2$ gain will generally not be possible. Instead, as noted in [23], the $\mathcal L_2$ -gain like property enforced is

$$\int_{0}^{T} \|y_{d}(t)\|^{2} dt < 2\gamma^{2} \int_{0}^{T} \|u_{\text{lin}}(t)\|^{2} dt + \beta$$
 (11)

for all $T \in [0, \infty)$ and some $\beta > 0$. Despite not being a "true" \mathcal{L}_2 gain, it appears that minimizing the bound γ is useful.

Stability, interpreted in the foregoing generalized sense, and performance are guaranteed using the quadratic Lyapunov functions and the \mathcal{L}_2 gain like property in Eq. (11). The following lemma, which uses elements from the results of [13,23], was assembled as the starting point for the analysis.

Lemma 1: Consider the following well-posed dynamic system:

$$S \sim \begin{cases} \dot{x} &= f(x, w) \\ z &= h(x, w) \end{cases}$$

where $f(\cdot,\cdot):\mathbb{R}^n\times\mathbb{R}^m\mapsto\mathbb{R}^n$ and $h(\cdot,\cdot):\mathbb{R}^n\times\mathbb{R}^m\mapsto\mathbb{R}^p$, and well-posedness is taken in the sense discussed in Remark 1. Consider a quadratic Lyapunov function $V(x)=x'P_1x$; sets $\mathcal{E}(P_1)$ and $\mathcal{E}(P_2)$; and positive scalars $\tau_1,\ \tau_2,\ \epsilon$, and γ . Assume that the following inequality holds for all $x\neq 0$, and w

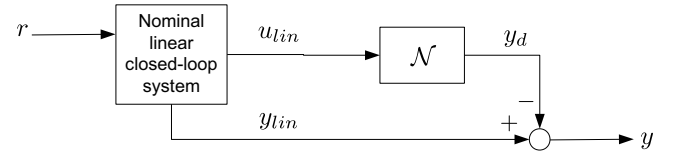


Fig. 4 Mismatch system where the nonlinear dynamic system \mathcal{N} is presented in Eq. (10).

$$\dot{V}(x) + \epsilon V(x) + \frac{1}{\gamma} ||z||^2 - \gamma ||w||^2 + \tau_1 (1 - x' P_1 x)$$

$$+ \tau_2 (x' P_2 x - 1) < 0$$
(12)

and assume further that $P_2 > P_1$ and $\tau_2 > \tau_1$. Then, the following

- 1) When w = 0, for all $x(0) \in \mathcal{E}(P_1)$, the state x(t) converges to the smallest level set containing $\mathcal{E}(P_2)$ in finite time.
- 2) When w is such that $||w||_{2,[0,T]} \le s/\sqrt{2\gamma}$, s < 1, and $||w(t)||^2 \ge$ $(\tau_2 - \tau_1)/\gamma$ for all $t \in [0, T]$, then
 - a) $x(t) \in \mathcal{E}(P_1)$ for all $t \in [0, T]$, and
 - b) the following \mathcal{L}_2 gain condition holds:

$$\int_0^T \|z(t)\|^2 dt < 2\gamma^2 \int_0^T \|w(t)\|^2 dt + \beta$$
 (13)

Proof: The proof is similar to Lemma 1 in [23] with modifications accounting for the local behavior of the system:

- 1) When $w = 0, x \in \mathcal{E}(P_1)$, and $x \notin \mathcal{E}(P_2)$, inequality (12) implies simply that $\dot{V}(x) + \epsilon V(x) < 0$, which means that the state converges exponentially to the smallest level set containing the set $\mathcal{E}(P_2)$.
 - 2) Inequality (12) can be rearranged as

$$\begin{split} \dot{V}(x) + \epsilon V(x) + \frac{1}{\gamma} \|z\|^2 - \gamma \|w\|^2 + (\tau_1 - \tau_2) + x'(\tau_2 P_2 - \tau_1 P_1) x < 0 \\ \Rightarrow \dot{V}(x) + \frac{1}{\gamma} \|z\|^2 - \gamma \|w\|^2 + (\tau_1 - \tau_2) + x'(\tau_2 P_2 - \tau_1 P_1) x < 0 \\ \Rightarrow \dot{V}(x) - \gamma \|w\|^2 + (\tau_1 - \tau_2) + x'(\tau_2 P_2 - \tau_1 P_1) x < 0 \end{split}$$

Because of the assumptions on P_2 and P_1 and τ_2 and τ_1 , this inequality implies

$$\dot{V}(x) < \gamma ||w||^2 + (\tau_2 - \tau_1)$$

Therefore, if $(\tau_2 - \tau_1)/\gamma \le ||w||^2$ on the interval [0, T], or equivalently $\tau_2 - \tau_1 \le \gamma ||w||^2$, then

$$\dot{V}(x) < 2\gamma ||w||^2$$

on this interval and integrating $V(x(T)) < s^2$, and thus, x(t) belongs to the ellipsoid $\mathcal{E}(P_1/s^2)$ over this interval. Since s < 1, this implies that, for w satisfying the conditions in the lemma, $x(T) \in \mathcal{E}(P_1)$. This

Returning to inequality (12), over the interval [0, T], it follows that

$$\begin{split} \dot{V}(x) + \epsilon V(x) + \frac{1}{\gamma} \|z\|^2 - \gamma \|w\|^2 + (\tau_1 - \tau_2) + x'(\tau_2 P_2 - \tau_1 P_1) x < 0 \\ \Rightarrow \dot{V}(x) + \frac{1}{\gamma} \|z\|^2 - \gamma \|w\|^2 + (\tau_1 - \tau_2) < 0 \end{split}$$

This implies that

$$\dot{V}(x) + \frac{1}{\gamma} \|z\|^2 < \gamma \|w\|^2 + \tau_2 - \tau_1 < 2\gamma \|w\|^2$$

Integrating this from [0, T] then gives Eq. (13). This is part 2.b.

The main result is obtained by applying Lemma 1 to system \mathcal{N} and adding the constraints in Sec. III.

Theorem 1: For a given scalar $\tau_1 > 0$, if there exist positive definite matrices Q_1 and Q_2 , a positive definite diagonal matrix U, diagonal matrices T_a and T_b , matrices $R_{a,4}$ and L, and positive scalars τ_2 and γ such that Eq. (18) and the linear matrix inequalities (20-22) are satisfied, then with $F = LQ_1^{-1}$, system (10) is such that

- 1) When $u_{lin} = 0, \forall x_a(0) \in \mathcal{E}(P_1)$, the state $x_a(t)$ converges to the smallest level set containing $\mathcal{E}(P_2)$ in finite time.

2) When $u_{\text{lin}} \neq 0$, the \mathcal{L}_2 gain like condition (11) holds. *Proof:* Using the system \mathcal{N} in Eq. (10) and the quadratic Lyapunov function $V(x_a) = x'_a P_1 x_a$, inequality (12) becomes

$$\begin{split} x_a'(P_1(A_p + B_p F) + (A_p + B_p F)'P_1)x_a + 2x_a'P_1B_p\tilde{u} \\ + \frac{1}{\gamma}\|y_d\|^2 - \gamma\|u_{\text{lin}}\|^2 + \tau_1(1 - x_a'P_1x_a) + \tau_2(x_a'P_2x_a - 1) < 0 \end{split}$$

Using Eq. (6) yields the bound:

$$x_{a}'(P_{1}(A_{p} + B_{p}F) + (A_{p} + B_{p}F)'P_{1})x_{a} + 2x_{a}'P_{1}B_{p}\tilde{u}$$

$$+ \frac{1}{\gamma}\|y_{d}\|^{2} - \gamma\|u_{\text{lin}}\|^{2} + \tau_{1}(1 - x_{a}'P_{1}x_{a}) + \tau_{2}(x_{a}'P_{2}x_{a} - 1)$$

$$+ 2\tilde{u}'W(u - r_{a} + r_{b} + r_{a}^{-} - r_{b}^{-} + \bar{u} - \tilde{u} + Hx_{a}) < 0$$
(14)

Then, using the shifted ramp function properties in Sec. III gives

$$x'_{a}(P_{1}(A_{p} + B_{p}F) + (A_{p} + B_{p}F)'P_{1})x_{a} + 2x'_{a}P_{1}B_{p}\tilde{u}$$

$$+ \frac{1}{\gamma}\|y_{d}\|^{2} - \gamma\|u_{\text{lin}}\|^{2} + \tau_{1}(1 - x'_{a}P_{1}x_{a}) + \tau_{2}(x'_{a}P_{2}x_{a} - 1)$$

$$+ 2\tilde{u}'W(u - r_{a} + r_{b} + r_{a}^{-} - r_{b}^{-} + \bar{u} - \tilde{u} + Hx_{a}) + \chi'M\chi$$

$$+ 2\chi'_{a}R_{a}(u - a - r_{a} + r_{a}^{-}) + 2\chi'_{b}R_{b}(u - b - r_{b} + r_{b}^{-})$$

$$+ 2r'_{a}T_{a}(r_{a} - (u - a)) + 2r'_{b}T_{b}(r_{b} - (u - b)) < 0$$
(15)

where $\chi_a = [1 \ x_a' \ r_a' \ r_a'']'$ and $\chi_b = [1 \ x_a' \ r_b' \ r_b^{-}]'$. Partitioning R_a as $R_a = [R_{a,1}' \ R_{a,2}' \ R_{a,3}' \ R_{a,4}']'$, where $R_{a,1} \in \mathbb{R}^{1 \times m}$, $R_{a,2} \in \mathbb{R}^{n \times m}$, and $R_{a,3}$, $R_{a,4} \in \mathbb{R}^{m \times m}$. Applying similar partitioning to R_b and partitioning M as $M = \operatorname{block}(M_{ii})$, where $i, j = 1, \dots, 5$. Majorizing inequality (15) then leads to the matrix inequality (16). This

$$\mathcal{M}_{11} = M_{11} - 2R_{a,1}a - 2R_{b,1}b + \tau_1 - \tau_2, \quad \mathcal{M}_{12} = -R_{a,1}F - R_{b,1}F - a'R'_{a,2} - b'R'_{b,2}$$

$$\mathcal{M}_{22} = P_1(A_p + B_pF) + (A_p + B_pF)'P_1 + \frac{1}{\gamma}C'_pC_p - (R_{a,2} + R_{b,2})F - F'(R_{a,2} + R_{b,2})' - \tau_1P_1 + \tau_2P_2$$
(16)

inequality contains the product of matrix variables, which cannot be resolved through standard techniques (e.g., Schur complements or congruence transformations). Therefore, choosing $R_{a,2} = F'R'_{a,4}$, $R_{b,2} = F'R'_{b,4}$, $R_{a,4} = T_a - R_{a,3}$, $R_{b,4} = T_b - R_{b,3}$, $R_{a,1} = -a'R_{a,4}$, $R_{b,1} = -b'R_{b,4}$, and $R_{a,4} = R'_{a,4} = R'_{b,4} = R'_{b,4}$, a congruence transformation blockdiag $(1, P_1^{-1}, W^{-1}, R_{a,4}^{-1}, I, \ldots, I)$ and Schur complements can be applied, which results in the matrix inequality (17), where $U = W^{-1}$, $Z = HQ_1$, and $L = FQ_1$.

Matrix inequality (17) is still not linear because of the nonlinear terms in the (2,2), (3,4), (4,3), (4,4), and (10,10) blocks.

$$\overline{\mathcal{M}}_{11} = M_{11} + 2a'R_{a,4}a + 2b'R_{a,4}b + \tau_1 - \tau_2, \qquad \mathcal{M}_{22} = A_pQ_1 + B_pL + Q_1A'_p + L'B'_p - \tau_1Q_1 + \tau_2Q_2$$

(17)

Therefore, to resolve this, in the (2,2) block element of Eq. (17) the nonlinear term $\tau_2 Q_2$ is replaced with Q_2 by imposing

$$\tau_2 < 1 \tag{18}$$

Likewise, the (3,4), (4,3), and (10,10) block elements of Eq. (17), which contain $R_{a,4}^{-1}$, and the (4,4) block element, which contains $-\gamma R_{a,4}^{-2}$, are replaced by linear block elements as follows. Define

$$\mathcal{R} := \begin{bmatrix} R_{a,4}^{-1} & R_{a,4}^{-1} \\ * & -\gamma R_{a,4}^{-2} \end{bmatrix} \equiv R_D^{-1} \bar{R} R_D^{-1} < -Y, \quad Y > 0$$
 (19)

where $R_D = \text{blockdiag}(R_{a,4}, R_{a,4}),$

$$\bar{R} = \begin{bmatrix} R_{a,4} & R_{a,4} \\ R'_{a,4} & -\gamma I_m \end{bmatrix}, \quad Y = \begin{bmatrix} Y_{11} & Y_{12} \\ * & Y_{22} \end{bmatrix}$$

and the block elements of Y conform with \mathcal{R} . The inequality in Eq. (19) is satisfied if the following is satisfied:

$$\begin{bmatrix} \bar{R} & R_D \\ R_D & -2I_{2m} + Y \end{bmatrix} < 0 \tag{20}$$

where Young's inequality $-Y^{-1} \le -2I + Y$ is used in this step [29]. Therefore, by imposing Eq. (20) and replacing the (3,4), (4,3), (4,4), and (10,10) block elements by $-Y_{12}$, $-Y_{21}$, $-Y_{22}$, and $-Y_{11}$, respectively, the linear matrix inequality (21) implies Eq. (17):

$$Q_1 < Q_2 \tag{22a}$$

$$\begin{bmatrix} Q_1 & Z_i' \\ Z_i & \delta T_i^2/s^2 \end{bmatrix} > 0 \quad \forall \ i \in \{1, 2, \dots, m\}$$
 (22b)

To ensure $\mathcal{E}(P_2) \subset \mathcal{E}(P_1)$ requires that $x_a'P_1x_a \leq x_a'P_2x_a \leq 1$ or equivalently, $P_2 - P_1 = Q_1^{-1}Q_2Q_1^{-1} - Q_1^{-1} \geq 0$, which is enforced by Eq. (22a). Finally, using the Schur complement, inequality (7) is satisfied by Eq. (22b).

To minimize the \mathcal{L}_2 gain and increase the region of stability [achieved by maximizing $\mathcal{E}(P_1)$ and the difference in volume between $\mathcal{E}(P_1)$ and $\mathcal{E}(P_2)$], the following optimization is executed with performance weights η_1, η_2 , and η_3 :

$$\min(\eta_1 \gamma - \eta_2(|Q_2| - |Q_1|) - \eta_3|Q_1|)$$

subject to Eqs. (18) and (20-22).

Remarkably, Theorem 1 enables one to design the AWC using linear matrix inequalities, despite the initial Lyapunov analysis in Eq. (15), which is somewhat complicated. From the solution to the optimization problem, the AWC gain is determined from $F = LQ_1^{-1}$, which is used in the implementation of Eq. (3).

\[\mathcal{M}_1 \] * * * * * * * * *	M ₂₂ * * * * * *	$\bar{u}'U$ $B_pU - L' + Z'$ $-2U$ * * * * *	2L' -Y ₁₂ -Y ₂₂ * * *	0 $-I$ $-I$ $M_{22} + 2R_{a,4}$ $*$ $*$	0 I I $M_{23} + T_a$ $-2R_{a,4}$ $M_{33} + 2R_{a,4}$ *	$M_{14} + 2b'R_{a,4}$ 0 I -I M_{24} M_{34} $M_{44} + 2R_{a,4}$ *	0 $-I$ I M_{25} M_{35} $M_{45} + T_b$ $-2R_{a,4}$ $M_{55} + 2R_{a,4}$	$0 \\ Q_1C'_p \\ 0 \\ 0 \\ 0 \\ 0 \\ 0 \\ 0 \\ 0$	0 0 0 0 0	< 0
*	*	*	*	*	*	*	$M_{55} + 2R_{a,4}$ *	0 –γI	0	
*	*	*	*	*	*	*	*	*	$-Y_{11}$	

 $\mathcal{M}_{11} = M_{11} + 2a'R_{a,4}a + 2b'R_{a,4}b + \tau_1 - \tau_2, \qquad \mathcal{M}_{22} = A_pQ_1 + B_pL + Q_1A'_p + L'B'_p - \tau_1Q_1 + Q_2$

V. Simulation Results

A planetary lander with the general architecture shown in Fig. 5 was considered, which are governed by the nonlinear rigid-body dynamics given by

$$\dot{x}_{p} = \left(I_{4} \otimes \begin{bmatrix} 0 & 1 \\ 0 & 0 \end{bmatrix}\right) x_{p} + \left(J_{a}^{-1} \otimes \begin{bmatrix} 0 \\ 1 \end{bmatrix}\right) T \phi(u) + g(x_{p}) \otimes \begin{bmatrix} 0 \\ 1 \end{bmatrix}$$
(23)

where $x_p = [z \ \dot{z} \ \theta_x \ \dot{\theta}_x \ \theta_y \ \dot{\theta}_z \ \dot{\theta}_z]', J_a = \mathrm{diag}(m_l, J_x, J_y, J_z),$ $g(x_p)$ is a nonlinear function consisting of cross-product terms and an Euler term for the gravitational force, and T is a mapping from thrust to generalized body forces given by

$$T = \begin{bmatrix} -\cos\theta_t & -\cos\theta_t & -\cos\theta_t & -\cos\theta_t \\ -d_y\cos\theta_t & d_y\cos\theta_t & d_y\cos\theta_t & -d_y\cos\theta_t \\ d_x\cos\theta_t & d_x\cos\theta_t & -d_x\cos\theta_t & -d_x\cos\theta_t \\ -\sin\theta_t & \sin\theta_t & -\sin\theta_t & \sin\theta_t \end{bmatrix}$$

The development of these dynamics is described in [21].

As depicted in Fig. 5, each corner of the lander had a thruster bank consisting of three thrusters. The thrusters were unidirectional on/off thrusters, each producing a mass-normalized thrust of 0.455 N/kg. The thrusters were tilted slightly toward each corner by a thrust tilt angle θ_t to provide the yaw forces. The lander was assumed to operate in the Martian gravitational field ($g=3.7 \text{ m/s}^2$). The vehicle parameters are listed in Table 1. The required thrust force for hover does not correspond to the available quantized thrust. Instead, each thruster bank must cycle between two and three thrusters.

The controller and AWC were designed from the linearized lander dynamics about the hover operating point $[g(x_p) = 0 \text{ in Eq. } (23)]$, and it was assumed that all states were measurable, $y = x_p$. The linearization of Eq. (23) resulted in a plant structure: $G(s) = \text{blockdiag}(G_1(s), \ldots, G_4(s))T$, which was a set of marginally stable double integrators with input coupling resulting from the thrust to generalized body force mapping matrix T. Therefore, following [21], the control signal was taken as $u = T^{-1}(u_{\text{lin}} - u_d)$, and the controller and AWC were structured, respectively, as $K(s) = \text{blockdiag}(K_1(s), \ldots, K_4(s))$ and $\Theta(s) = \text{blockdiag}(\Theta_1(s), \ldots, \Theta_4(s))T$. Then, if $\Theta_i(s)$ is designed via Theorem 1 to stabilize the ith plant–controller combination, the diagonally structured system is asymptotically stable.

Each $K_i(s)$ implemented full-state feedback control with reference tracking:

$$K_i(s) \sim \begin{cases} \dot{x}_c = C_r y_{\text{lin}} + r \\ u_{\text{lin}} = K_I x_c + K_x y_{\text{lin}} \end{cases}$$

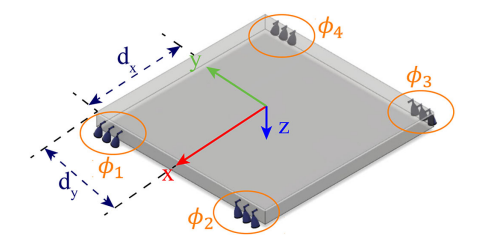


Fig. 5 General architecture of a planetary lander.

Table 1 Mass normalized landing vehicle parameters

Parameter	Variables	Values	Units
Mass	m_l	1.0	
Mass moment of inertia	$[J_x, J_y, J_z]$	[0.3, 0.3, 0.6]	m^2
Half-spans	d_x, d_y	2.5	m
Thrust tilt angle	θ_t	2.75	deg

where $C_r = [-1\ 0]$ such that $z_p = [z\ \theta_x\ \theta_y\ \theta_z]'$ are the tracked states, and K_I and K_x are integral and full-state feedback gains, respectively, designed such that the nominal closed-loop system poles lie at [-1,-1.5,-2] for each channel. The procedure implied by Theorem 1 was implemented to design each $\Theta_i(s)$ with $\tau_1 = 0.75, s = 1/25$, and $\eta = \tilde{\eta}/\sum \tilde{\eta}$, where $\tilde{\eta} = [5\ 300\ 200]$. The AWC synthesized using this approach is referred to as the proposed AWC.

For comparison, an AWC without the benefit of the ramp function properties given in Sec. III was designed with only the standard sector [0,I] constraints considered, that is, inequality (14) with r_a, r_a, r_b, r_b^- , and \bar{u} excluded, and like the proposed AWC design, Eqs. (18) and (22) were included in this design. The AWC synthesized by this approach is referred to as the sector [0,I] AWC. Table 2 lists the \mathcal{L}_2 gain upper bounds γ of the nonlinear mapping $\mathcal{N}: u_{\text{lin}} \mapsto y_d$. From this, we see that the less conservative ramp function constraints of the proposed method yield significantly less \mathcal{L}_2 gain bounds (four orders of magnitude lower than the bounds provided by the sector [0,I] design method). This performance outcome is reflected in the simulation results.

The design parameters described previously were used for all simulations. Likewise, the controller K(s) remained the same throughout. Finally, for the simulations presented, the full nonlinear dynamics (23) were included. Remark 4 provided at the end of this section summarizes the results when the nonlinear dynamics are excluded.

Figure 6 shows the response to a reference commanding the vehicle to decrease in altitude and roll about the three axes, whereas Fig. 7 illustrates the corresponding thrust produced by thruster bank ϕ_1 . (Note that similar characteristics were seen with the other thruster banks.) Without AWC, the vehicle was unable to follow the reference, and the thruster bank ϕ_1 remained saturated after 9 s. With the sector [0,I] AWC, the vehicle deviated considerably from the reference and eventually recovered after 40 s. Moreover, the performance of the thruster bank was unsatisfactory, as the entire bank of thrusters cycled between all thrusters on and all thrusters off. The proposed compensator was able to follow the reference (noting that the slowest closed-loop time constant was 1 s), and the thruster bank cycled between two and three thrusters upon reaching a steady state. This is the appropriate cycling for hover.

Of additional interest is the steady-state error of the vehicle's vertical position $e_{z,ss} = r_{z,\infty} - z_{ss}$. Although $e_{z,ss} = 0$ for the sector [0, I] AWC, it does so at the cost of on/off cycling of all the thrusters. In contrast, a nonzero $e_{z,ss}$ existed for the proposed method. By synthesizing a more localized compensator, the steady-state error can be reduced. Choosing s = 1/250 for both sector [0, I] and the proposed compensator resulted in the responses shown in Fig. 8 and the thrusts shown in Fig. 9. Although there is some minor improvement to the response with the sector [0, I] AWC, the notable improvement is in the steady-state error for the response with the proposed compensator. Similar to the previous case with s = 1/25, the thrust with the sector [0, I] AWC had unsatisfactory performance, cycling between all thrusters on and all thrusters off, whereas the thrust with the proposed compensator design cycled between two and three thrusters (appropriate cycling for hover) upon reaching a steady state.

To emphasize the capability of AWC to manage quantization, the number of thrusters per thruster bank was increased to six. Figure 10 illustrates the response to reference commands similar to the previous case, whereas Fig. 11 illustrates the corresponding thrust produced by thruster bank ϕ_1 . (As in the previous case, similar characteristics were observed with the other thruster banks.)

Table 2 \mathcal{L}_2 gain upper bounds γ of nonlinear mapping $\mathcal{N}: u_{1\text{in}} \mapsto y_d$

		Channels				
Compensator	1	2	3	4		
Proposed Sector [0, I]	12 19e4	119 216e4	119 216e4	33 58e4		

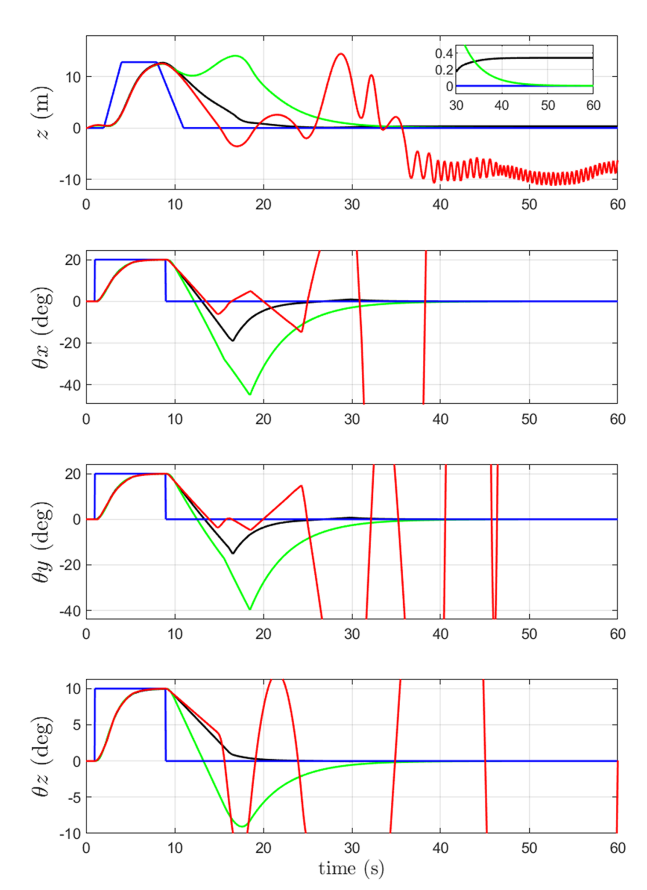


Fig. 6 Response with three thrusters per thruster bank (s=1/25): — reference; —, without antiwindup; —, with sector [0,I] antiwindup; —, with the proposed antiwindup.

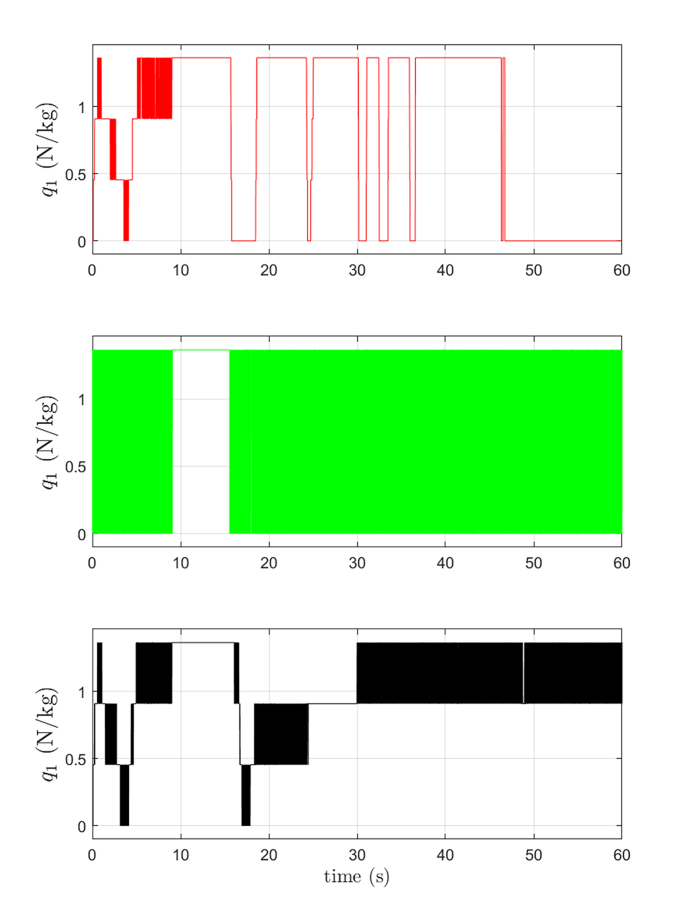


Fig. 7 Thrust with three thrusters per thruster bank (s=1/25); —, without antiwindup; —, with sector [0,I] antiwindup; —, with the proposed antiwindup.

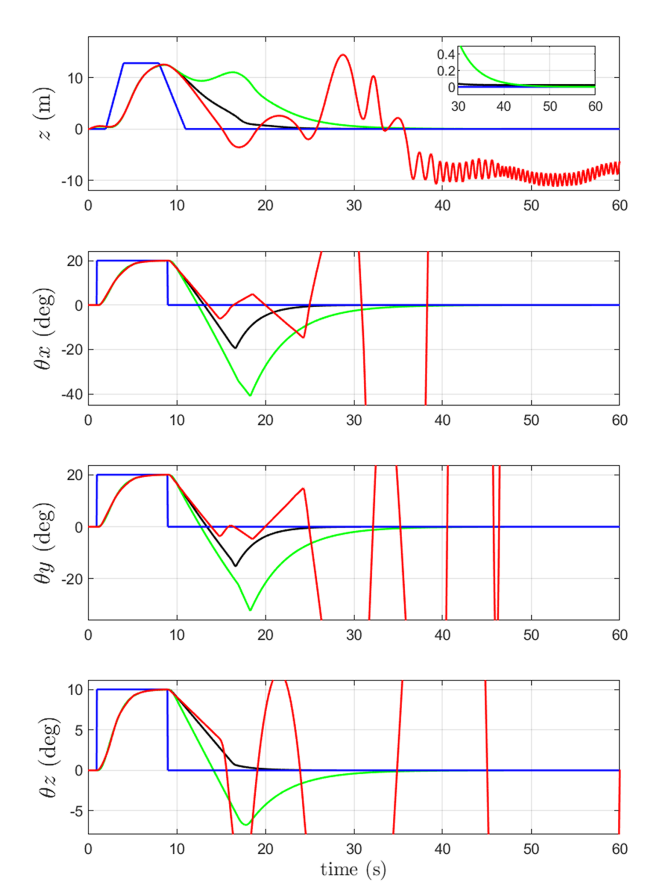


Fig. 8 Response with three thrusters per thruster bank (s=1/250): —, reference; —, without antiwindup; —, with sector [0,I] antiwindup; —, with the proposed antiwindup.

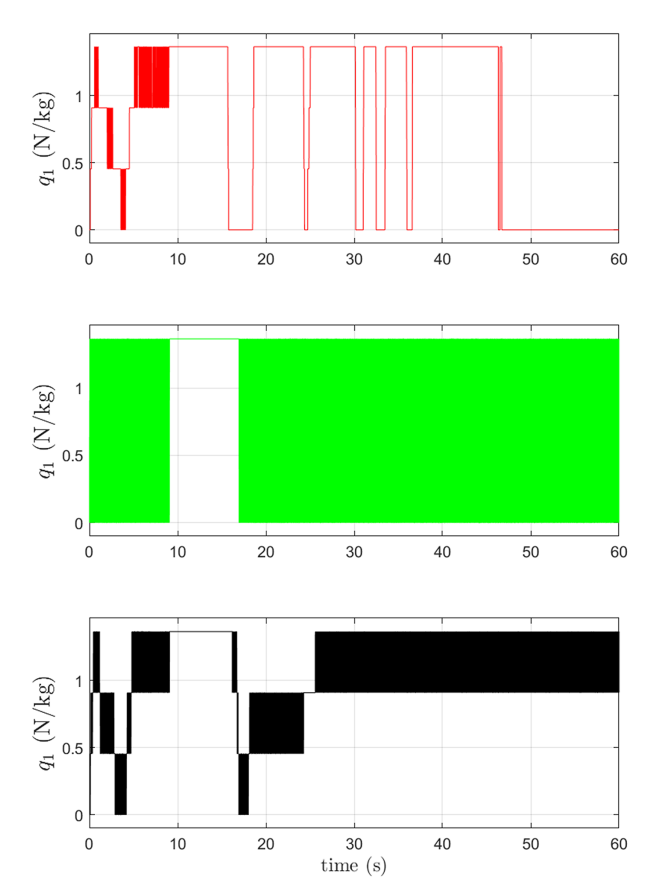


Fig. 9 Thrust with three thrusters per thruster bank (s=1/250): —, without antiwindup; —, with sector [0,I] antiwindup; —, with the proposed antiwindup.

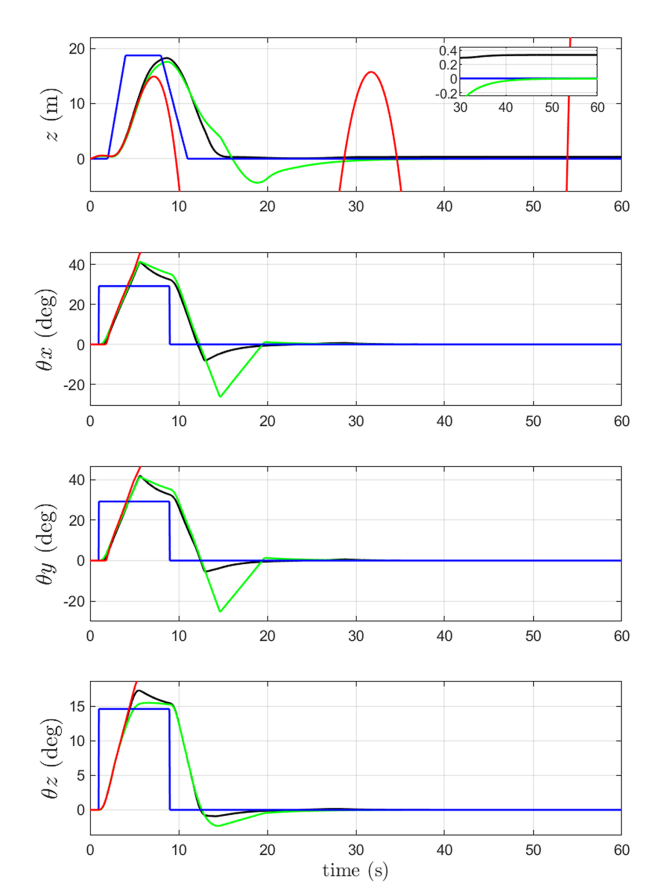


Fig. 10 Response with six thrusters per thruster bank (s=1/25): —, reference; —, without antiwindup; —, with sector [0, I] antiwindup; —, with the proposed antiwindup.

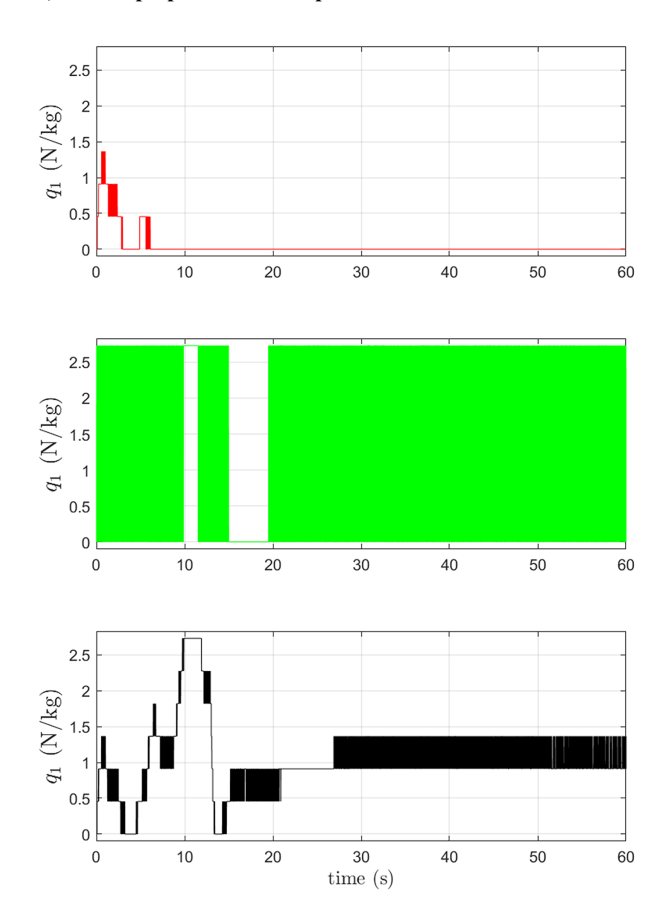


Fig. 11 Thrust with six thrusters per thruster bank (s = 1/25): —, without antiwindup; —, with sector [0, I] antiwindup; —, with the proposed antiwindup.

Without AWC the vehicle was unable to follow the reference, and the thrust remained saturated after 6 s. With the sector [0, I] AWC (s=1/25), the vehicle deviated from the reference and eventually settled after 40 s. In addition, similar to the previous case, the thruster bank illustrated unsatisfactory control as the entire thruster bank cycled between all thrusters on and all thrusters off. Although some deviation was present with the proposed antiwindup (s=1/25), this deviation and the settling time were considerably less than those of the sector [0,I] AWC. Once a steady state was achieved, where again a nonzero $e_{z,ss}$ occurred, the thruster banks cycled between two and three thrusters after 25 s, which is the appropriate cycling for hover.

To minimize the steady-state error of the proposed method, a more localized compensator was again synthesized (s=1/250). Using this value for both sector [0,I] and the proposed method resulted in the responses and thrusts shown in Figs. 12 and 13, respectively. Although an improved performance was achieved with the sector [0,I] compensator, this approach was outperformed by the proposed approach, which also had zero steady-state error. Similar to the previous simulation cases, the thrust of the proposed approach exhibited a preferred behavior. It should be emphasized that while response performance is critical for accurate navigation of the vehicle, maintaining the proper thrust is equally important for practical reasons: minimizing fuel consumption and wear on the thrusters.

Remark 4: Simulations with the lander dynamics linearized about the hover operating point $(g(x_p) = 0 \text{ in Eq. } [23)]$ were executed. The performance of the vehicle response was comparable for the sector [0,I] AWC and the proposed method. However, the thrusts of the sector [0,I] AWC continued to have undesirable behavior, fluctuation between all thrusters off and all thrusters on. In fact, this full-off and full-on fluctuation occurs even when saturation can be prevented using all thrust levels (see Fig. 14 for an example response and Fig. 15 for the corresponding thrust). Note that all thrust levels were used

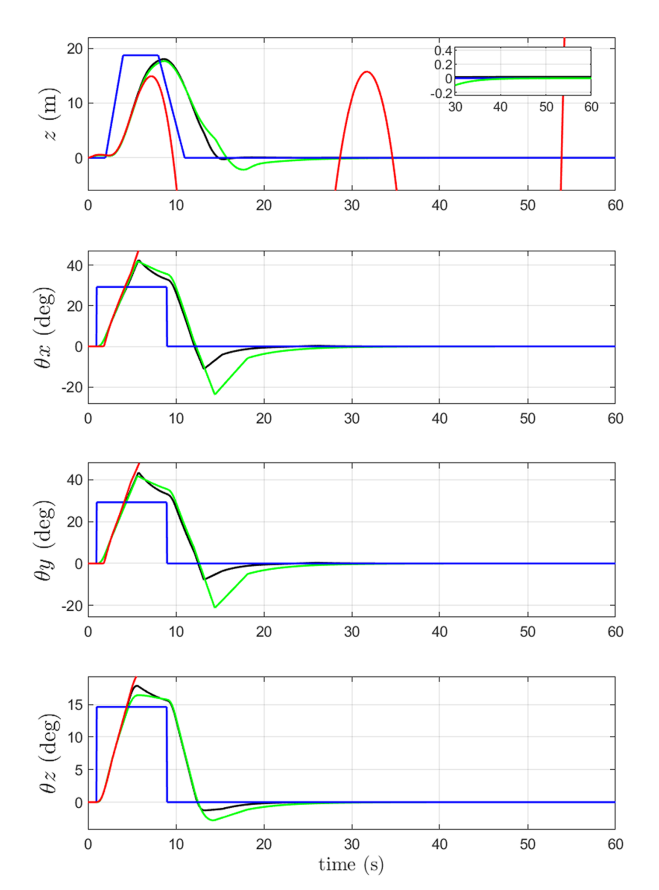


Fig. 12 Response with six thrusters per thruster bank (s=1/250): —, reference; —, without antiwindup; —, with sector [0, I] antiwindup; —, with the proposed antiwindup.

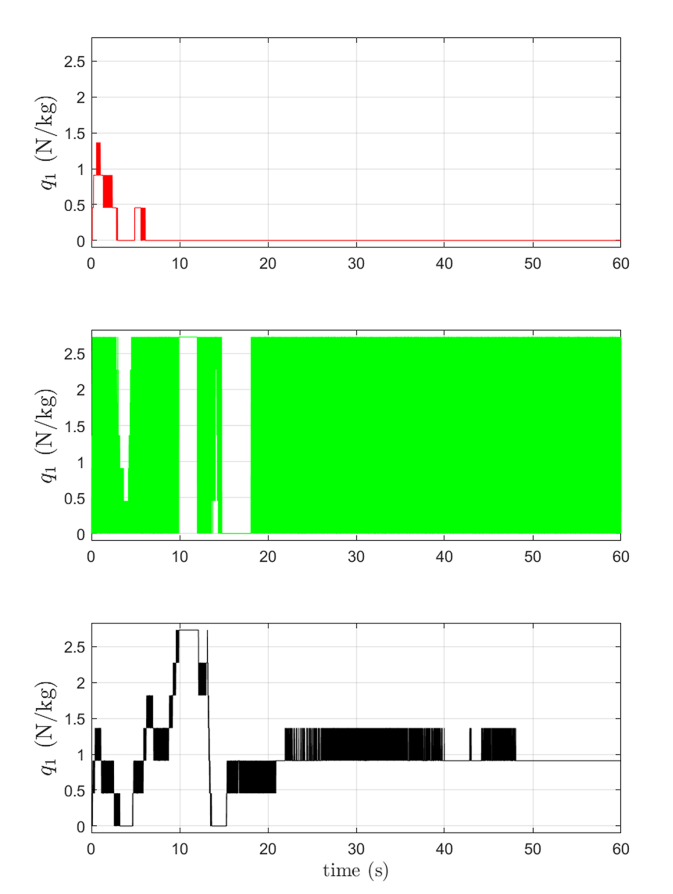


Fig. 13 Thrust with six thrusters per thruster bank (s = 1/250): —, without antiwindup; —, with sector [0, I] antiwindup; —, with the proposed antiwindup.

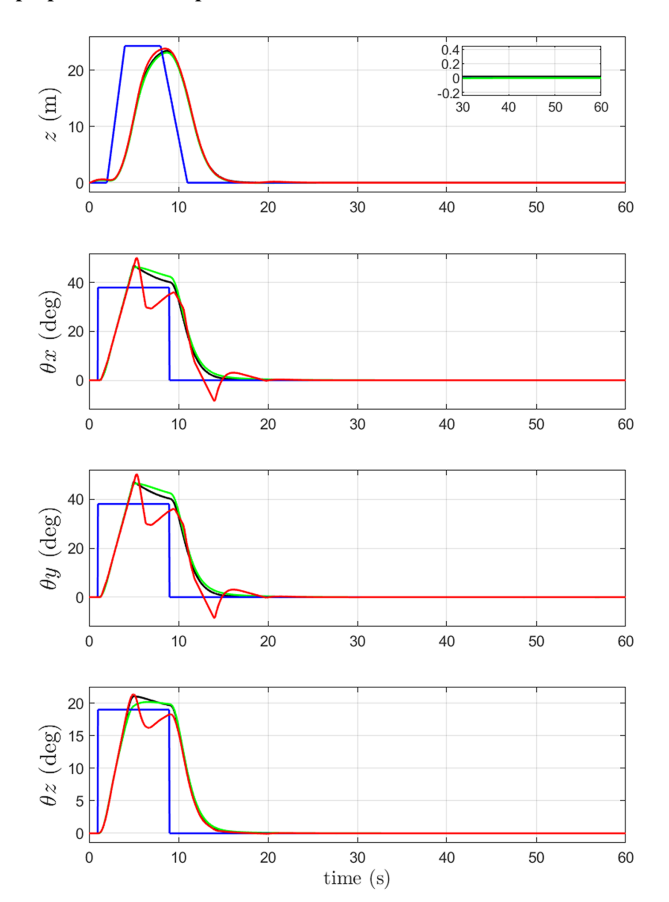
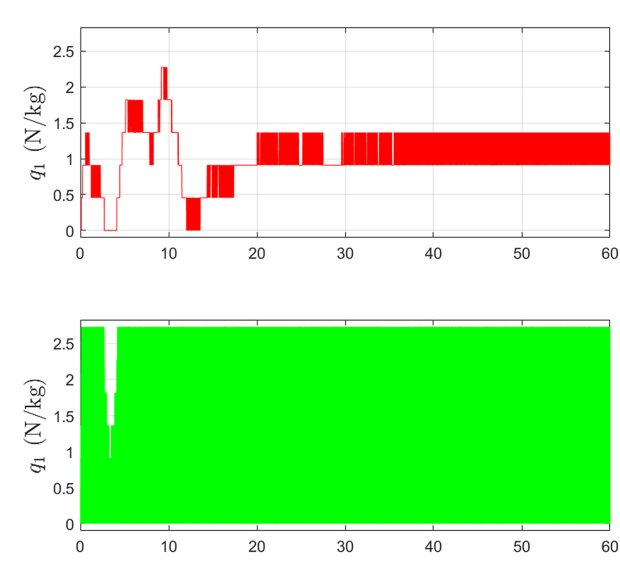


Fig. 14 Linearized response with six thrusters per thruster bank (s = 1/250): —, reference; —, without antiwindup; —, with sector [0, I] antiwindup; —, with the proposed antiwindup.



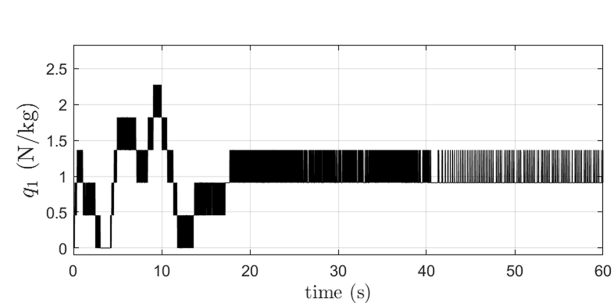


Fig. 15 Thrust of the linearized lander with six thrusters per thruster bank (s = 1/250): —, without antiwindup; —, with sector [0, I] antiwindup; —, with the proposed antiwindup.

when AWC was absent and when the proposed method was implemented. Saturation was avoided in both cases, and the response was improved using the proposed approach.

VI. Conclusions

An antiwindup design method was developed for systems subject to input quantization and saturation. The salient features of this study are as follows: 1) the AWC synthesis conditions are framed as linear matrix inequalities; 2) ramp functions have been exploited to obtain less conservative bounds on the control-signal error compared with a standard sector bound; and 3) the results are applicable to rigid-body systems, which was the motivation for this study. A key outcome is that the design method provides a significant reduction in \mathcal{L}_2 gain bound compared with a standard sector antiwindup design. This approach is transferable to many nontraditional control problems (e.g., drug delivery, which is often inherently quantized, and environmental management, which is often quota-based), as well as to traditional control fields where quantization is intrinsic (network control, communications, and event-triggered control systems). Because practical quantized actuation systems may suffer from limited switch rate, a future study will explore extensions that address issues resulting from the finite rate of switching. The simultaneous controller and AWC design will also be investigated to explore their potential in expanding the region of stability.

Acknowledgments

This study was supported by the National Science Foundation (award CMMI-2137030) and the UKRI Engineering and Physical Sciences Research Council (grant number EP/X012654/1).

References

- Brockett, R. W., and Liberzon, D., "Quantized Feedback Stabilization of Linear Systems," *IEEE Transactions on Automatic Control*, Vol. 45, No. 7, 2000, pp. 1279–1289. https://doi.org/10.1109/9.867021
- [2] Orphee, J., Hannan, M., Braden, E., Anzalone, E., Ahmed, N., Craig, S., Olson, N., Everett, J., and Miller, K., "Guidance, Navigation, & Control for NASA Lunar Pallet Lander," *American Astronautical Society Annual Guidance, Navigation and Control Conference*, American Astronautical Soc., Springfield, VA, 2019, pp. 117–128.
- [3] Delchamps, D. F., "Stabilizing a Linear System with Quantized State Feedback," *IEEE Transactions on Automatic Control*, Vol. 35, No. 8, 1990, pp. 916–924. https://doi.org/10.1109/9.58500
- [4] Azuma, S., and Sugie, T., "Synthesis of Optimal Dynamic Quantizers for Discrete-Valued Input Control," *IEEE Transactions on Automatic Control*, Vol. 53, No. 9, 2008, pp. 2064–2075. https://doi.org/10.1109/TAC.2008.929400
- [5] Azuma, S., and Sugie, T., "Stability Analysis of Quantized Feedback Systems Including Optimal Dynamic Quantizers," 2008 47th IEEE Conference on Decision and Control, Inst. of Electrical and Electronics Engineers, New York, 2008, pp. 3392–3397. https://doi.org/10.1109/CDC.2008.4738662
- [6] Gonçalves, J. M., Megretski, A., and Dahleh, M. A., "Global Stability of Relay Feedback Systems," *IEEE Transactions on Automatic Control*, Vol. 46, No. 4, 2001, pp. 550–562. https://doi.org/10.1109/9.917657
- [7] Ahn, K., and Yokota, S., "Intelligent Switching Control of Pneumatic Actuator Using On/Off Solenoid Valves," *Mechatronics*, Vol. 15, No. 6, 2005, pp. 683–702. https://doi.org/10.1016/j.mechatronics.2005.01.001
- [8] Kalman, R., "Nonlinear Aspects of Sampled-Data Control Systems," Proceedings of Symposium Nonlinear Circuit Analysis VI, Polytechnic Inst. of Brooklyn, Brooklyn, NY, 1956, pp. 273–313.
- [9] Bullo, F., and Liberzon, D., "Quantized Control via Locational Optimization," *IEEE Transactions on Automatic Control*, Vol. 51, No. 1, 2006, pp. 2–13. https://doi.org/10.1109/TAC.2005.861688
- [10] Salton, A. T., Flores, J. V., Zheng, J., and Fu, M., "Asymptotic Tracking of Discrete-Time Systems Subject to Uniform Output Quantization," *IEEE Control Systems Letters*, Vol. 7, Dec. 2022, pp. 829– 834
- https://doi.org/10.1109/LCSYS.2022.3226702
 [11] Fu, M., and Xie, L., "The Sector Bound Approach to Quantized Feedback Control," *IEEE Transactions on Automatic Control*, Vol. 50, No. 11, 2005, pp. 1698–1711. https://doi.org/10.1109/TAC.2005.858689
- [12] Elia, N., and Mitter, S. K., "Stabilization of Linear Systems with Limited Information," *IEEE Transactions on Automatic Control*, Vol. 46, No. 9, 2001, pp. 1384–1400. https://doi.org/10.1109/9.948466
- [13] Tarbouriech, S., and Gouaisbaut, F., "Control Design for Quantized Linear Systems with Saturations," *IEEE Transactions on Automatic Control*, Vol. 57, No. 7, 2011, pp. 1883–1889. https://doi.org/10.1109/TAC.2011.2179845
- [14] Hindi, H., and Boyd, S., "Analysis of Linear Systems with Saturation Using Convex Optimization," *Proceedings of the 37th IEEE Conference on Decision and Control (Cat. No. 98CH36171)*, Vol. 1, Inst. of Electrical and Electronics Engineers, New York, 1998, pp. 903–908. https://doi.org/10.1109/CDC.1998.760808

- [15] Zaccarian, L., and Teel, A. R., Modern Anti-Windup Synthesis: Control Augmentation for Actuator Saturation, Vol. 36, Princeton Univ. Press, Princeton, NJ, 2011.
- [16] Groff, L., Valmorbida, G., and da Silva, J. M., "Stability Analysis for Piecewise Affine Discrete-Time Systems," 2019 IEEE 58th Conference on Decision and Control (CDC), Inst. of Electrical and Electronics Engineers, New York, 2019, pp. 8172–8177. https://doi.org/10.1109/CDC40024.2019.9029638
- [17] Valmorbida, G., and Ferrante, F., "On Quantization in Discrete-Time Control Systems: Stability Analysis of Ternary Controllers," 2020 59th IEEE Conference on Decision and Control (CDC), Inst. of Electrical and Electronics Engineers, New York, 2020, pp. 2543–2548. https://doi.org/10.1109/CDC42340.2020.9304125
- [18] Ferrante, F., and Valmorbida, G., "Stability Analysis of a Class of Discontinuous Discrete-Time Systems," *IEEE Control Systems Letters*, Vol. 7, June 2022, pp. 454–459. https://doi.org/10.1109/LCSYS.2022.3183937
- [19] Turner, M. C., Herrmann, G., and Postlethwaite, I., "Incorporating Robustness Requirements into Antiwindup Design," *IEEE Transactions on Automatic Control*, Vol. 52, No. 10, 2007, pp. 1842–1855. https://doi.org/10.1109/TAC.2007.906185
- [20] Mulder, E. F., Kothare, M. V., and Morari, M., "Multivariable Anti-Windup Controller Synthesis Using Linear Matrix Inequalities," *Automatica*, Vol. 37, No. 9, 2001, pp. 1407–1416. https://doi.org/10.1016/S0005-1098(01)00075-9
- [21] Richards, C. M., and Turner, M. C., "Combined Static and Dynamic Anti-Windup Compensation for Quadcopters Experiencing Large Disturbances," *Journal of Guidance, Control, and Navigation*, Vol. 43, No. 4, 2020, pp. 673–684. https://doi.org/10.2514/1.G004575
- [22] Bernstein, D. S., and Michel, A. N., "A Chronological Bibliography on Saturating Actuators," *International Journal of Robust and Nonlinear Control*, Vol. 5, No. 5, 1995, pp. 375–380. https://doi.org/10.1002/rnc.4590050502
- [23] Sofrony, J., and Turner, M., "Anti-Windup Design for Systems with Input Quantization," 2015 54th IEEE Conference on Decision and Control (CDC), Inst. of Electrical and Electronics Engineers, New York, 2015, pp. 7586–7591. https://doi.org/10.1109/CDC.2015.7403418
- [24] Alsamadi, S., Ferrante, F., and Tarbouriech, S., "Anti-Windup-Like Compensator Synthesis for Discrete-Time Quantized Control Systems," *IFAC-PapersOnLine*, Vol. 55, No. 25, 2022, pp. 43–48. https://doi.org/10.1016/j.ifacol.2022.09.321
- [25] Richards, C., and Turner, M., "Anti-Windup Compensation for Stable and Unstable Systems with Quantized and Saturated Inputs," 2023 American Control Conference (ACC), Inst. of Electrical and Electronics Engineers, New York, 2023, pp. 1396–1401. https://doi.org/10.23919/ACC55779.2023.10156408
- [26] Cortes, J., "Discontinuous Dynamical Systems," *IEEE Control Systems*, Vol. 28, No. 3, 2008, pp. 36–73. https://doi.org/10.1109/MCS.2008.919306
- [27] Hu, T., and Lin, Z., Control Systems with Actuator Saturation: Analysis and Design, Birkhäuser Verlag, Basel, 2001. https://doi.org/10.1007/978-1-4612-0205-9
- [28] Teel, A. R., and Kapoor, N., "The L₂ Anti-Windup Problem: Its Definition and Solution," 1997 European Control Conference (ECC), Inst. of Electrical and Electronics Engineers, New York, 1997, pp. 1897–1902. https://doi.org/10.23919/ECC.1997.7082381
- [29] Cao, Y. Y., Sun, Y. X., and Cheng, C., "Delay-Dependent Robust Stabilization of Uncertain Systems with Multiple State Delays," *IEEE Transactions on Automatic Control*, Vol. 43, No. 11, 1998, pp. 1608–1612.